Journal of Engineering Mathematics (2006) 54: 99–118
DOI 10.1007/s10665-005-9017-y

Inviscid instability of an unbounded shear layer: effect of surface tension, density and velocity profile

SAAD ALABDULJALIL and ROGER H. RANGEL
Department of Mechanical and Aerospace Engineering, University of California, Irvine, CA 92697-3975, USA (E-mail: rhrangel@uci.edu)

Received 15 March 2003; accepted in revised form 26 August 2005 / Published online: 9 December 2005

Abstract. The inviscid temporal stability analysis of an unbounded shear layer of two fluids of different density is investigated. Two background velocity profiles are considered: the piecewise-linear profile and the more realistic error-function profile. The disturbance kinetic energy is analyzed to physically understand the mechanism that causes instability. The surface-tension effect is investigated extensively. Surface tension is found to destabilize the neutrally stable waves that exist when surface tension is absent. This surface-tension-induced unstable mode is generally weaker than the dominant mode and extremely less evident when the density and/or viscosity difference increases. Short-wavelength instability is observed with a background viscosity jump at the interface. A comparison between the two velocity profiles is presented. The piecewise-linear profile does not match the more realistic results obtained with the error-function profile in the short wavelength range, especially in nonhomogeneous shear-layer flows; however, the phase-speed results are in a good agreement with those of the error-function profile.

Key words: Kelvin-Helmholtz instability, shear layer, surface tension

1. Introduction

Under certain conditions, free-shear-layer flows become inviscidly unstable to infinitesimal disturbances. At sufficiently large Reynolds numbers, the inviscid framework is adequate to describe the evolution of perturbations in free flows such as jets and layers [1]. Furthermore, the inviscid limit can be used in a shear flow consisting of a viscous and an inviscid fluid. Early work by Miles [2] showed that for a flow in which the light fluid is inviscid and the dense fluid is viscous, the viscosity has little effect on the instability. The results of Lindsay [3] agree with this conclusion.

The inviscid problem of an infinite surface of discontinuity, *i.e.*, vortex sheet, separating two unbounded fluids of different density and velocity, and subjected to an initial sinusoidal disturbance of infinitesimal amplitude was first recognized by Helmholtz in 1868, and solved by Kelvin in 1871. This type of flow is found to be always unstable as long as a velocity difference exists. Also, it experiences the largest growth rate in a homogeneous fluid, *i.e.*, no density discontinuity.

Zalosh [4] used the discrete-vortex method to study the stabilizing effect of the surface tension on the vortex-sheet evolution. His results revealed that at the intermediate surface-tension range, the flow is marginally stable, and for large values the flow is stable. In the marginally stable configuration, the amplitude grows slightly at first and then oscillates in time.

The role of surface tension and density difference in the instability of the vortex sheet is extensively discussed by Rangel and Sirignano [5]. The inclusion of the surface tension is shown to temporarily slow down the rollup rate of the vortex sheet. When the surface-tension

force is large enough, the accumulation of vorticity at the interface is prevented and consequently the rollup disappears.

Vortex-sheet profiles cannot persist, being diffused by viscosity into continuously varying shear layers. The study of such discontinuous profiles is therefore based on the expectation that they retain characteristic features of continuous shear-layer profiles, while allowing simpler mathematical treatment. This is indeed so, but care is required in interpreting the results. Thus, continuous profiles give more realistic results but require more complicated treatment.

Drazin and Howard [6] obtained formulas to determine the instability characteristics of unbounded parallel inviscid flows in the limit of long waves. These formulas are valid for any arbitrary velocity profile since the detailed structure of the profile is not important for small wavenumbers. A three-term-approximation power series for the hyperbolic-tangent profile was derived.

Michalke [7] computed the eigenfunctions and the amplified eigenvalues spectrum of the hyperbolic-tangent profile numerically using a shooting technique. The dimensionless cut-off wavenumber was found to be 1; however, this neutral wavenumber was already known analytically by Garcia [8]. The numerical results were in a good agreement with the three-term approximation by Drazin and Howard [6] up to $\alpha = 0{\cdot}2$.

An inviscid damping mode for the hyperbolic-tangent profile was found by Tatsumi *et al.* [9] in the higher range of wavenumbers ($\alpha > 1$). They showed that the only mechanism that could consume the kinetic energy of the disturbance in this inviscid limit is the consideration of a smooth continuous velocity profile. Such a profile implies the existence of viscosity in the basic flow, and obviously this viscosity retains its role as a hidden parameter to damp these inviscid disturbances.

Pouliquen *et al.* [10] carried out a detailed investigation of the inviscid instability of two immiscible fluids in a shear layer when the thickness of the density profile is much smaller than the thickness of the velocity profile. Although the perturbation analysis ignores the viscosity effects, the chosen velocity profile satisfies the continuation of the shear stress at the interface. With a symmetric broken-line profile, counter-propagating (Holmboe) waves were observed. When the profile symmetry is broken relatively high wavenumbers were dominated by a single propagating mode moving in the same direction as the less viscous fluid. The linear stability for an inviscid density-stratified shear layer is well documented in Redekopp [11] with more emphasis on environmental flows.

2. Rayleigh's equation

The instability eigenvalue problem on the interval $-\infty < y < \infty$ for inviscid parallel shear flows is defined by the Rayleigh's equation:

$$\phi'' - \alpha^2 \phi - \frac{U''}{U - c} = 0, \tag{1}$$

where α is a real positive wavenumber, c is the complex wave speed, $U(y)$ is the background velocity and the prime denotes differentiation with respect to y. The eigenfunction $\phi(y)$ is an unknown complex function that represents the normal mode amplitude of the disturbance stream function:

$$\psi'(x, y, t) = \phi(y) e^{i\alpha(x - ct)}. \tag{2}$$

From Equations (2), one can obtain the following expressions for the complex amplitude of the disturbance velocities:

$$\hat{u}(y) = \phi'(y), \tag{3a}$$

$$\hat{v}(y) = -\mathrm{i}\alpha\phi(y), \tag{3b}$$

It can be seen that Equation (1) is unchanged when α is replaced by $-\alpha$. Thus, if we take $\alpha \geq 0$, there exists a solution with $c_i > 0$ for instability to occur. Therefore $c_i > 0$, can be considered as the criterion for instability [12, Section 21].

The boundary condition for the disturbance ϕ is that the disturbance velocities must vanish at infinity:

$$\phi(\infty) = \phi(-\infty) = 0. \tag{4}$$

Note that all the variables in this paper are dimensionless, unless otherwise stated.

3. Temporally developing viscous shear layers

Although we are investigating the inviscid instability of the flow, it is of interest to examine, in some approximate way, the role that viscosity may play, not during the development of the instability, but in the background flow whose stability we are trying to analyze. In this regard, it is useful to consider the similarities and differences between spatially developing viscous shear layers and temporally developing ones. In both cases, we are dealing with a viscous region that grows, with downstream distance in the former case or with time in the latter one. Thus, the notion of non-parallelism that exists in the spatially developing layer has its counterpart in the temporal case, except that it is the time variation itself, as opposed to being frozen in time, that represents the analogy. Therefore, considering a frozen state of the flow in the temporally developing layer is akin to assuming parallel flow in the spatially developing problem.

Of course, there are important mathematical differences between the two flows. While, in the temporal flow, we only deal with a simple parabolic evolution of the equations, in the spatially developing flow we have both convection and diffusion in the direction of development. This difference is important if only for the fact the temporally developing layer admits an exact solution in the form of an error-function while the spatially developing layer does not have an exact solution, although the hyperbolic tangent profile is a reasonable approximation under the parallel-flow assumption. Furthermore, the temporally growing shear layer admits an exact error-function solution in the case where the upper and lower streams have different but constant densities and viscosities.

In Section 6 we examine the temporal instability of this error-function profile by making a "frozen flow" approximation as described above. However, we first investigate the instability of an approximation to such solution as represented by a piecewise-linear profile in Section 5 after analyzing the kinetic energy behavior in Section 4.

4. Kinetic energy of disturbances

The energy contained within the disturbance is fed by the background flow. Thus, in order to understand the evolution of the disturbance and the role of surface tension, we investigate the mechanism of this energy transfer between the background flow and the disturbance motion. To derive the disturbance kinetic-energy equation, we multiply the x- and y-components of

the nonlinear inviscid two-dimensional equations of motion for the disturbance by u' and v', respectively. The two equations are then added and integrated over one wavelength ($2\pi/\alpha$) of the disturbance and a domain bounded by $y = \pm\infty$.

Care must be taken when integrating terms involving the pressure over the y-domain. This integration should be carried out for the upper and lower domains separately, as the pressure is discontinuous across the interface due to surface tension.

Let the initial displacement of the interface due to a small disturbance amplitude ϵ be

$$\eta(x,t) = \epsilon e^{i\alpha(x-ct)}. \tag{5}$$

Accordingly, the pressure balance at the interface can be expressed as follows:

$$p_2'(0) - s p_1'(0) = s\epsilon\alpha^2 W e^{i\alpha(x-ct)}. \tag{6}$$

W is the inverse of the Weber number and is defined as:

$$W = \frac{\sigma}{\rho_1 L_c^* (V_c^*)^2}, \tag{7}$$

where the asterisks denote dimensional quantities. It should be pointed out that we neglect gravity effects in this analysis. This is a valid assumption in small-scale applications such as atomizers and spray jets.

Upon utilizing integration by parts and the periodicity behavior of the perturbation velocity along with the results in (6), one can obtain the equation governing the kinetic energy of the disturbance:

$$\begin{aligned}\frac{\partial}{\partial t}\int_0^{\infty}\int_0^{2\pi/\alpha} \tfrac{1}{2} s\left(u_1'^2 + v_1'^2\right) \mathrm{d}x\mathrm{d}y + \frac{\partial}{\partial t}\int_{-\infty}^{0}\int_0^{2\pi/\alpha} \tfrac{1}{2}\left(u_2'^2 + v_2'^2\right) \mathrm{d}x\mathrm{d}y \\ = s\int_0^{\infty}\int_0^{2\pi/\alpha} (-u_1'v_1')\frac{\mathrm{d}U}{\mathrm{d}y}\mathrm{d}x\mathrm{d}y + \int_{-\infty}^{0}\int_0^{2\pi/\alpha} (-u_2'v_2')\frac{\mathrm{d}U}{\mathrm{d}y}\mathrm{d}x\mathrm{d}y - \pi s\alpha^2 W\phi_{oi} e^{2\alpha c_i t}.\end{aligned} \tag{8}$$

where ϕ_{oi} is the imaginary part of the disturbance eigenfunction at the interface.

The left-hand side of (8) is the temporal variation of the disturbance kinetic energy. It involves a balance between the production term (first two terms on the right-hand side) and the surface-tension energy (last term on the right-hand side). The appearance of W in the surface-tension energy term shows that surface tension plays an important role in the stability mechanism of the flow. When surface tension is sufficiently large, such that its effect is greater than that of the Reynolds stress, the flow is stable.

To get further insight into the effect of the surface tension, it seems more meaningful to evaluate the integrals in (8) over the wavelength. Upon decomposing the perturbation velocity based on the normal-mode solution and after a considerable amount of manipulation, we can rewrite Equation (8) as:

$$\begin{aligned}c_i s\int_0^{\infty}\left(|\phi_1'|^2 + \alpha^2|\phi_1|^2\right)\mathrm{d}y + c_i\int_{-\infty}^{0}\left(|\phi_2'|^2 + \alpha^2|\phi_2|^2\right)\mathrm{d}y \\ = s\int_0^{\infty}\left(\phi_{1r}\phi_{1i}' - \phi_{1i}\phi_{1r}'\right)\frac{\mathrm{d}U}{\mathrm{d}y}\mathrm{d}y + \int_{-\infty}^{0}\left(\phi_{2r}\phi_{2i}' - \phi_{2i}\phi_{2r}'\right)\frac{\mathrm{d}U}{\mathrm{d}y}\mathrm{d}y - s\alpha^2 W\phi_{oi}.\end{aligned} \tag{9}$$

where $|\phi|$ denotes the modulus of ϕ.

Equation (9) describes the balance between the time rate of change of the kinetic energy of disturbances with the work done by the Reynolds stress and the surface-tension energy. This equation is general for any background velocity profile. It can be seen from Equation (9) that,

if the Reynolds stress term is positive, which means that the energy is being transferred to the disturbance flow, and larger than the surface tension term, we have unstable flow. Further, when the flow is unstable, *i.e.*, $c_i > 0$, the second term on the right-hand side of (9) is always negative; surface tension appears to always have a stabilizing influence in the presence of growing disturbances. However, this is not always the case, as we will show in Section 7.

The destabilizing role of surface tension is best illustrated as a mathematical feature of the instability using the phase shift concept that was first discussed by Prandtl [13]. The amplitude of the normal mode for the perturbation velocities can be expressed in the form:

$$\hat{u}(y) = \left|\hat{u}(y)\right| \mathrm{e}^{\mathrm{i}\chi_u(y)}, \tag{10a}$$

$$\hat{v}(y) = \left|\hat{v}(y)\right| \mathrm{e}^{\mathrm{i}\chi_v(y)}, \tag{10b}$$

Upon averaging over a wavelength of the disturbance along with using Equations (3), the Reynolds stress appearing in the kinetic energy equation can be written as:

$$\tau_{xy} = -\overline{u'v'} = \tfrac{1}{4}\mathrm{i}\alpha(\phi\ \phi'^{\star} - \phi^{\star}\phi')\mathrm{e}^{2\alpha c_i t}, \tag{11}$$

where the bar and star denote, respectively, a spatial average quantity and a complex conjugate. Using (10) we can write the Reynolds stress as:

$$\tau_{xy} = -\overline{u'v'} = -\tfrac{1}{2}\left|\hat{u}(y)\right|\left|\hat{v}(y)\right|\cos[\chi_u(y) - \chi_v(y)]\mathrm{e}^{2\alpha c_i t}. \tag{12}$$

In the absence of surface tension, Equation (9) implies that, for neutrally stable waves, the Reynolds stress τ_{xy} must be zero and hence the phase-angle difference for the disturbance velocities in Equation (12) must be $\pm\pi/2$. Setting W to a nonzero value while keeping other flow parameters unchanged, shifts the phase angle difference to the unstable (second and third) quadrants in which the cosine of this difference is negative. This shift leads to a positive Reynolds stress which is large enough to overcome the otherwise stabilizing effect of surface tension and rendering these otherwise neutrally stable waves unstable.

5. Piecewise-linear profile

We consider two unbounded parallel streams of respective velocity V_1^* and V_2^*. The two streams are assumed to have different density ρ. Although we investigate the inviscid stability of the flow, we consider velocity distributions that satisfy, either in approximate or exact manner, the viscous equation for the background flow. The frame of reference is moving with a velocity $\frac{1}{2}\left(V_1^* + V_2^*\right)$. Upon taking the thickness of the background flow in the upper stream δ_1^* as the characteristic length and half the velocity discontinuity $V_c^* = \frac{1}{2}\left(V_1^* - V_2^*\right)$ as the characteristic velocity, we can express the piecewise-linear velocity profile as:

$$U(y) = \begin{cases} 1, & y > 1 \\ u_o + (1-u_o)y, & 0 < y < 1 \\ u_o + (1+u_o)\dfrac{y}{d}, & -d < y < 0 \\ -1, & y < -d \end{cases}, \tag{13}$$

where $d = \sqrt{s/m}$. If we define $s = \rho_1/\rho_2$ as the density ratio, $m = \mu_1/\mu_2$ as the viscosity ratio and $p = 1/\sqrt{sm}$, the dimensionless velocity of the interface is $u_o = (1-p)/(1+p)$.

The continuity of the vertical velocity at any point in the flow constitutes the kinematic condition. This condition requires that the vertical disturbance velocity between each subdomain must be equal:

$$\phi^{y^+} = \phi^{y^-}, \quad \phi^{y_o^+} = \phi^{y_o^-} = \epsilon(c - u_o), \tag{14}$$

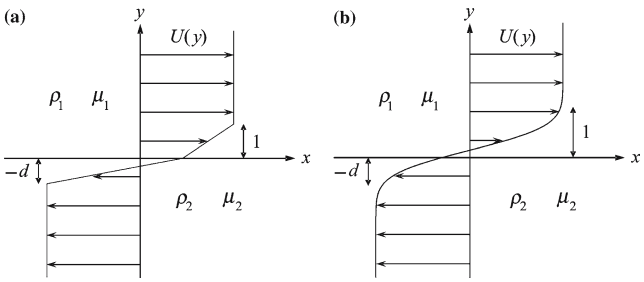

Figure 1. The basic flow. (a) Piecewise-linear profile, (b) error-function profile.

where the superscripts y^+ and y^- refer to the upper and lower side of y-subdomain at 1 and $-d$, while the subscript y_o refers to the interface (Figure 1).

The dynamic condition requires that the pressure must be equal on either side at $y=1$ and $-d$:

$$\left[U'\phi-(U-c)\phi'\right]^{y^+}=\left[U'\phi-(U-c)\phi'\right]^{y^-}. \tag{15}$$

Now we consider the dynamic condition at the interface where surface tension will be taken into account:

$$\left[\phi_2'(0)-s\phi_1'(0)\right](c-u_o)+\left[d^{-1}(1+u_o)\phi_2(0)-s(1-u_o)\phi_1(0)\right]=\epsilon s\alpha^2 W. \tag{16}$$

Upon solving Rayleigh's equation in (1) along with the boundary conditions in (4), one is led to:

$$\phi(y)=\begin{cases} A\mathrm{e}^{-\alpha y}, & y>1 \\ B\sinh(\alpha y)+G\cosh(\alpha y), & 0<y<1 \\ D\sinh(\alpha y)+E\cosh(\alpha y), & -d<y<0 \\ F\mathrm{e}^{\alpha y}, & y<-d \end{cases}. \tag{17}$$

We use the kinematic conditions in (14) along with the dynamic condition in (15) to solve for the constants in (17). This allows us to determine the dispersion equation for this flow by employing the dynamic condition at the interface:

$$\frac{2}{1+p}\left(\frac{1}{d}-d\right)(c-u_o)+\alpha\left(\tilde{D}-s\tilde{B}\right)(c-u_o)^2=s\alpha^2 W, \tag{18}$$

where $\tilde{B}$ and $\tilde{D}$ are constants defined as follows:

$$\tilde{B}=\frac{B}{\epsilon\,(c-u_o)}=-\frac{(c-1)\alpha\mathrm{e}^{\alpha}+(1-u_o)\cosh\alpha}{(c-1)\alpha\mathrm{e}^{\alpha}+(1-u_o)\sinh\alpha}, \tag{19a}$$

$$\tilde{D}=\frac{D}{\epsilon\,(c-u_o)}=\frac{(1+c)\alpha d\mathrm{e}^{\alpha d}-(1+u_o)\cosh(\alpha d)}{(1+c)\alpha d\mathrm{e}^{\alpha d}-(1+u_o)\sinh(\alpha d)}. \tag{19b}$$

Equation (18) gives a quartic equation in c. However, the case of homogeneous shear flow has a relatively simpler biquadratic equation for c:

$$\left[\frac{2\mathrm{e}^{-4\alpha}+8\alpha^2c^2-2(1-2\alpha)^2}{4\alpha^2c^2-(1-\mathrm{e}^{-2\alpha}-2\alpha)^2}\right]c^2=\alpha W. \tag{20}$$

Equations (18) and (20) are analogous to Equations (4) and (5) derived by Pouliquen *et al.* [10].

The temporal change of disturbances kinetic energy for a piecewise-linear profile can be obtained from the general Equation (9):

$$c_i s \int_0^\infty \left(|\phi_1'|^2 + \alpha^2 |\phi_1|^2\right) \mathrm{d}y + c_i \int_{-\infty}^0 \left(|\phi_2'|^2 + \alpha^2 |\phi_2|^2\right) \mathrm{d}y$$
$$= s(1-u_o) \int_0^1 \left(\phi_{1r}\phi_{1i}' - \phi_{1i}\phi_{1r}'\right) \mathrm{d}y + d^{-1}(1+u_o) \int_{-d}^0 \left(\phi_{2r}\phi_{2i}' - \phi_{2i}\phi_{2r}'\right) \mathrm{d}y - s\alpha^2 W c_i, \quad (21)$$

where $\phi_{oi} = c_i$ was used from the kinematic condition (14).

Integrating the Reynolds stress term on the right-hand side of (21) analytically using the solution in (17) we obtain:

$$c_i s \int_0^\infty \left(|\phi_1'|^2 + \alpha^2 |\phi_1|^2\right) \mathrm{d}y + c_i \int_{-\infty}^0 \left(|\phi_2'|^2 + \alpha^2 |\phi_2|^2\right) \mathrm{d}y$$
$$= s\alpha(1-u_o)(B_i c_r - B_r c_i) + \alpha(1+u_o)(D_i c_r - D_r c_i) - s\alpha^2 W c_i, \quad (22)$$

where B_r, B_i, D_r and D_i are the real and imaginary parts of the constants in (17).

Equation (21) shows that both fluids contribute towards the Reynolds shear stress acting on the background flow which controls the process of the energy transfer from and to the disturbances. Most of the time, the less viscous fluid generates the greatest part of the Reynolds stress that causes instability to occur.

6. Error-function profile

The analytical solution for a temporally growing shear-layer of two viscous semi-infinite fluids moving with uniform but different parallel velocities is used to determine the velocity profile in this problem. Accordingly, the dimensionless velocity of the upper and lower fluid in a shear-layer flow can be expressed, respectively, as follows:

$$U(y) = \begin{cases} \dfrac{2p}{1+p}\mathrm{erf}\,(y) + u_o, & y > 0 \\ \dfrac{2}{1+p}\mathrm{erf}\left(\dfrac{y}{d}\right) + u_o, & y < 0 \end{cases}. \quad (23)$$

The frame of reference is moving with the average velocity $\frac{1}{2}(V_1^* + V_2^*)$. Half of the difference between the free stream velocities in both fluids $\frac{1}{2}(V_1^* - V_2^*)$ was used to nondimensionalize the velocity. The parameters shown in Equation (23), p and d, and the interface velocity u_o are the same as defined in Section 5.

To proceed with the solution, it is convenient to replace the boundary conditions in (4) with the asymptotic behavior of the complex eigenfunction ϕ. This can be obtained by solving the Rayleigh's equation in the limit $y = \pm\infty$:

$$\text{as } y \longrightarrow \infty, \qquad \phi = C_1 \mathrm{e}^{-\alpha y} \quad \text{and} \quad \phi' = -\alpha\phi, \quad (24a)$$
$$\text{as } y \longrightarrow -\infty, \qquad \phi = C_2 \mathrm{e}^{\alpha y} \quad \text{and} \quad \phi' = \alpha\phi. \quad (24b)$$

Two interfacial conditions must be satisfied. The continuity of the normal velocity:

$$\phi_1(0) = \phi_2(0) = \epsilon(c - u_o) \quad (25)$$

and the pressure balance by surface tension:

$$\left[\phi_2'(0) - s\phi_1'(0)\right](c-u_o) + \frac{4}{\sqrt{\pi}(1+p)}\left[d^{-1}\phi_2(0) - d\phi_1(0)\right] = \epsilon s\alpha^2 W. \tag{26}$$

Introducing a new dependent variable f for the Rayleigh's equation such that:

$$\phi = \epsilon(c-u_o)\exp\left(\int_0^y f\,\mathrm{d}\tilde{y}\right) \tag{27}$$

and substituting (27) in Rayleigh's equation, we obtain:

$$f' = \alpha^2 - f^2 + \frac{U''}{U-c}. \tag{28}$$

The differential equation in (28) must be solved numerically in order to evaluate the eigenvalue c_i and thus determine the stability characteristics of the flow. To simplify the numerical computation and reduce the integration region to a finite interval, we transform the independent variable in Rayleigh's equation y as follows:

$$z = \begin{cases} 1 - \mathrm{e}^{-y}, & 0 \le y \le \infty \\ \mathrm{e}^{y/d} - 1, & -\infty \le y \le 0 \end{cases}. \tag{29}$$

Substituting Equations (23) and (29) in the transformed Rayleigh equation in (28) and breaking the resulting system of differential equations into real and imaginary parts yield the corresponding stability equations at each fluid region. For the upper fluid:

$$\frac{\mathrm{d}f_{1r}}{\mathrm{d}z} = \frac{\alpha^2 - f_{1r}^2 + f_{1i}^2}{1-z} + \frac{8p\log(1-z)\,\mathrm{e}^{-[-\log(1-z)]^2}}{\sqrt{\pi}\,(1-z)\,(1+p)} \times \frac{2p\,(1+p)^{-1}\,\mathrm{erf}[-\log(1-z)] + u_o - c_r}{\left\{2p\,(1+p)^{-1}\,\mathrm{erf}[-\log(1-z)] + u_o - c_r\right\}^2 + c_i^2}, \tag{30a}$$

$$\frac{\mathrm{d}f_{1i}}{\mathrm{d}z} = \frac{-2f_{1r}f_{1i}}{1-z} + \frac{8p\left[\sqrt{\pi}\,(1-z)\,(1+p)\right]^{-1}\log(1-z)\,\mathrm{e}^{-[-\log(1-z)]^2}c_i}{\left\{2p\,(1+p)^{-1}\,\mathrm{erf}[-\log(1-z)] + u_o - c_r\right\}^2 + c_i^2} \tag{30b}$$

and for the lower fluid:

$$\frac{\mathrm{d}f_{2r}}{\mathrm{d}z} = \frac{\alpha^2 - f_{2r}^2 + f_{2i}^2}{\mathrm{d}^{-1}(1+z)} - \frac{8\log(1+z)\,\mathrm{e}^{-[\log(1+z)]^2}}{\sqrt{\pi}\mathrm{d}\,(1+z)\,(1+p)} \times \frac{2\,(1+p)^{-1}\,\mathrm{erf}[\log(1+z)] + u_o - c_r}{\left\{2\,(1+p)^{-1}\,\mathrm{erf}[\log(1+z)] + u_o - c_r\right\}^2 + c_i^2}, \tag{31a}$$

$$\frac{\mathrm{d}f_{2i}}{\mathrm{d}z} = \frac{-2f_{2r}f_{2i}}{\mathrm{d}^{-1}(1+z)} + \frac{8\left[\sqrt{\pi}\mathrm{d}\,(1+z)\,(1+p)\right]^{-1}\log(1+z)\,\mathrm{e}^{-[\log(1+z)]^2}c_i}{\left\{2\,(1+p)^{-1}\,\mathrm{erf}[\log(1+z)] + u_o - c_r\right\}^2 + c_i^2}. \tag{31b}$$

Accordingly, the boundary conditions in (24) turn into:

$$\begin{aligned} f_{1r}(1) &= -\alpha, & f_{1i}(1) &= 0, \\ f_{2r}(-1) &= \alpha, & f_{2i}(-1) &= 0, \end{aligned} \tag{32}$$

where subscripts r and i denote the real and imaginary parts, respectively.

Equations (30) and (31) are undetermined at $z=1$ and -1 respectively. L'Hôpital's rule is used to evaluate the limiting values:

$$\left.\frac{\mathrm{d}f_{1r}}{\mathrm{d}z}\right|_{z\to 1} = \left.\frac{\mathrm{d}f_{1i}}{\mathrm{d}z}\right|_{z\to 1} = \left.\frac{\mathrm{d}f_{2r}}{\mathrm{d}z}\right|_{z\to -1} = \left.\frac{\mathrm{d}f_{2i}}{\mathrm{d}z}\right|_{z\to -1} = 0. \tag{33}$$

Combining the kinematic and dynamic conditions in (25) and (26) along with the transformation in (27) yields the following equation, which will be used as a required condition in the numerical computation:

$$\frac{4\left(d^{-1}-d\right)}{\sqrt{\pi}\,(1+p)}(c-u_o)+[f_2(0)-sf_1(0)](c-u_o)^2 = s\alpha^2 W. \tag{34}$$

The eigenvalue c is computed by integrating (30) and (31) numerically with a fourth-order Runge-Kutta method. An optimization algorithm developed by the authors that utilizes a parallelogram in the c_r-c_i-plane is used. The results are presented in Section 7.

From Equation (9), the disturbance kinetic energy for the error-function profile can be written as follows:

$$\begin{aligned} c_i s \int_0^1 (1-z)^{-1}\left(\left|\frac{\mathrm{d}\phi_1}{\mathrm{d}z}\right|^2+\alpha^2|\phi_1|^2\right)\mathrm{d}z + c_i\int_{-1}^0 (1+z)^{-1}\left(\left|\frac{\mathrm{d}\phi_2}{\mathrm{d}z}\right|^2+\alpha^2|\phi_2|^2\right)\mathrm{d}z \\ = \frac{4\mathrm{d}}{\sqrt{\pi}\,(1+p)}\int_0^1 \frac{\mathrm{e}^{-[-\log(1-z)]^2}}{(1-z)}\left(\phi_{1r}\frac{\mathrm{d}\phi_{1i}}{\mathrm{d}z}-\phi_{1i}\frac{\mathrm{d}\phi_{1r}}{\mathrm{d}z}\right)\mathrm{d}z \\ + \frac{4}{\sqrt{\pi}\,(1+p)}\int_{-1}^0 \frac{\mathrm{e}^{-[\log(1+z)]^2}}{(1+z)}\left(\phi_{2r}\frac{\mathrm{d}\phi_{2i}}{\mathrm{d}z}-\phi_{2i}\frac{\mathrm{d}\phi_{2r}}{\mathrm{d}z}\right)\mathrm{d}z - s\alpha^2 W c_i. \end{aligned} \tag{35}$$

7. Results and discussion

7.1. Homogeneous shear flow ($s=m=1$)

In this case, the shear flow is assumed to be homogeneous in terms of density and the background flow satisfies the equations for homogenous viscosity. When surface tension is set to zero, unstable and damped waves exist for wavenumbers under the cut-off wavenumber $\alpha_c = 0{\cdot}639$ for the piecewise-linear profile and 1·037 for the error-function profile, while traveling stable waves exist for $\alpha > \alpha_c$. It is worth noting that the results for a homogeneous error-function with no surface tension have a fair agreement with the results of Michalke [7] for the hyperbolic-tangent velocity profile. He found that the hyperbolic-tangent profile has a cut-off of 1 compared with 1·037 for the error-function and a maximum growth rate of 0·19 occurs at an optimum wavenumber of 0·445 compared with 0·216 and 0·485, respectively.

When the flow is homogeneous and the velocity profile is antisymmetric with respect to the cross-stream direction, it follows from [14] that the phase speed c_r is constant and equals the interface velocity u_o provided the unstable eigenfunction ϕ is unique. Consequently, we only need to iterate the eigenvalue c_i during the numerical computation which reduces the time required for convergence substantially.

In addition, we note that a neutrally stable stationary wave (a trivial solution of the equations) is also possible but usually ignored. This neutrally stable solution can be seen clearly in the error-function profile where the required condition at the interface (34) reduces to:

$$[f_2(0)-sf_1(0)](c-u_o)^2 = 0. \tag{36}$$

Obviously, a neutrally stable eigenvalue, $c_i = 0$, is a possible solution for all wavenumbers as long as the interface curvature is ignored. Although this trivial solution is ignored in the

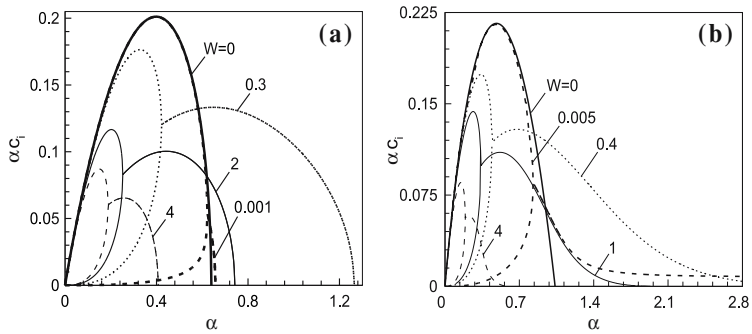

Figure 2. Dimensionless disturbance growth rate αc_i vs. the dimensionless wavenumber α for a homogeneous shear layer with different surface-tension values. (a) Piecewise-linear profile, (b) error-function profile.

$W=0$ analysis, it plays a major role when surface tension is added. Imposing surface tension at $y=0$ is found to perturb this neutral wave away from its neutrally stable state and, as a result, a new set of damped and unstable modes is created. These new modes eventually merge with the original modes at a certain wavenumber α_m as shown in Figure 2. This is analogous to the observation made by Yih [15] that introducing a viscosity stratification in a shear layer creates new unstable modes in the neighborhood of a hidden neutral mode for the case of a same fluid. This second unstable mode with $W \neq 0$ can be seen to arise from Equation (20) which produces a bi-quadratic equation in c:

$$\hat{A}c^4 + \hat{B}c^2 + \hat{D} = 0, \tag{37}$$

where the coefficients are defined as follows:

$$\hat{A} = 8\alpha^2, \quad \hat{B} = 2e^{-4\alpha} - 2(1-2\alpha)^2 - 4\alpha^3 W, \quad \hat{D} = \left(1 - e^{-2\alpha} - 2\alpha\right)^2 \alpha W. \tag{38}$$

When the surface tension is of the order of ε, where ε is a very small quantity, Equation (37) gives the following roots:

$$c_{1,2} = \pm i\sqrt{\frac{\hat{B}}{\hat{A}}}, \quad c_{3,4} = \pm i\sqrt{\frac{\varepsilon}{4\hat{A}\hat{B}^2}}. \tag{39a,b}$$

The corresponding eigenvalues to (39a) are unstable for all $\alpha < \alpha_c$ where $\hat{B}$ changes sign after the cut-off wavenumber. On the other hand, the roots in (39b) are unstable for all $\alpha < \alpha_m$ where the two modes merge and the first mode dominates. When the surface tension is neglected, the roots in (39b) become trivial solutions to (37), which represent the neutral stable waves that are observed in $W=0$ case.

For the error-function profile, the real part of the required condition at the interface, Equation (34), shows that when the two fluids are identical, then for $\alpha < \alpha_m$ the complex wave speed c has a quadratic equation with discriminant equal to $-4[f_{2r}(0) - f_{1r}(0)]\alpha^2 W$ which produces the first unstable mode. On the other hand, the imaginary part of the required condition gives the second unstable mode as long as $f_{2i}(0) - f_{1i}(0) = 0$. However, when $\alpha > \alpha_m$, the difference between the real parts of the transformed eigenfunctions at the interface,

$f_{2r}(0) - f_{1r}(0)$, changes sign and becomes negative and the difference in the imaginary parts become non-zero which in turn eliminates one of the complex roots, leaving only one unstable mode thereafter.

The appearance of this mode can be attributed to the slip in the tangential disturbance velocity that is caused by the surface tension at the interface. In this sense, it may be concluded that surface tension, while stabilizing the most unstable mode, introduces instability in a previously neutral mode. A mathematical argument for this phenomenon was given at the end of Section 4. To explain this phenomenon physically, we employ the kinematic condition in (14) with the dynamic condition in (16) (or alternatively (25) and (26) for the error-function profile) to obtain:

$$c\left[\hat{u}(0^-) - \hat{u}(0^+)\right] = \epsilon\alpha^2 W. \tag{40}$$

The presence of surface tension generates an additional discontinuity in the tangential velocity at the interface. This instability is proportional to the square of the wavenumber, which explains the rapid growth of the second mode with increasing wavenumber, as seen in Figure 2, especially when W is sufficiently large. When $W = 0$, no slip in the tangential velocity occurs and the second mode is neutrally stable. This is analogous to the situation involving neutrally stable waves in the Kelvin-Helmholtz problem, where the instability is driven by the discontinuity of two uniform velocity profiles at the interface. When an additional velocity difference is imposed, those neutrally stable waves become unstable.

The kinetic energy equation in (8) shows the important role that surface tension plays in the stabilizing mechanism of the flow. When W is sufficiently large, such that the last term in (8) is larger than the Reynolds stress integrals, the flow is stable to all waves. Conversely, when W is not large enough to overcome all the energy produced by the Reynolds stress, the disturbances keep growing and the flow becomes unstable. Based on this argument, we expect a critical W to exist above which surface tension stabilizes all wavenumbers. Figure 2 shows that in a certain range of W, surface tension actually destabilizes progressively shorter waves until W exceeds a critical value of 2·383 for the piecewise-linear profile and 1·931 for the error-function profile, where the cut-off wavenumber becomes exactly the same as the no-surface-tension cut-off. For all $W > W_c$ surface tension was observed to stabilize all wavenumbers.

It is clear from (8) that, in order to have unstable flow, there must be a dominant region in the flow where the Reynolds stress $(-u'v')$ has the same sign as the velocity gradient of the background flow $(\mathrm{d}U/\mathrm{d}y)$. Otherwise the disturbance energy will decrease and eventually a stable flow results. Accordingly, we do not expect surface tension to work only as a stabilizing factor because the Reynolds stress would not be able to develop the appropriate sign in case of a stable flow when surface tension is absent.

As pointed out in Section 4, this destabilizing effect can be attributed to the slight shift, caused by surface tension, in the phase difference for the disturbance velocities outside the stable quadrants. This increases the work done by the Reynolds stress on the background flow such that its destabilizing influence dominates over the stabilizing effect of surface tension. To better understand the indirect impact of surface tension on the Reynolds stress, it is of interest to integrate the Reynolds stress term in Equation (21) analytically for the $s = m = 1$ case:

$$\int_{-1}^{1} \left(\phi_i \phi_r' - \phi_r \phi_i'\right) \mathrm{d}y = \frac{2\alpha^2 c_i |c|^2}{\alpha^2\left(c_i^2 + \vartheta^2\right)\mathrm{e}^{2\alpha} + 2\alpha\vartheta\mathrm{e}^{\alpha}\sinh(\alpha) + \sinh^2(\alpha)}, \tag{41}$$

where ϑ equals $(c_r - 1)$, respectively. The kinetic energy of the disturbances as a function of wavenumber is plotted in Figure 3(a). Further, Equations (35) are integrated numerically to evaluate the temporal change of disturbances energy for the error-function profile. The results are shown in Figure 3(b). These figures show that, at low to intermediate W, surface tension contributes to boost the kinetic energy of the least unstable disturbed waves (the lower branch) making them more unstable and it also delivers energy to some otherwise neutrally stable waves in the $0{\cdot}6 < \alpha < 1{\cdot}25$ range for the linear profile and $1{\cdot}04 < \alpha < 1{\cdot}8$ for the error-function profile, making them unstable. For the most unstable waves (the upper branch of the bi-modal region) surface tension does exhibit the expected stabilizing effect as the last term in Equation (9) overcomes the destabilizing effect of the Reynolds stress. It is also interesting to notice from Figure 3 that, although large values of W $(W > 2)$ supply more kinetic energy to the intermediate range of disturbed waves $(0{\cdot}1 < \alpha < 0{\cdot}75)$, these waves become less unstable as most of that energy is used to speed up the traveling disturbances rather than to intensify the growth rate. This gain in the velocity of the disturbances as W increases can be seen in Figure 4.

A very interesting phenomenon in the solution of the piecewise-linear profile can be seen in Figure 5. A second unstable region can exist beyond a certain stable range of wavenumbers. The second instability region is small compared with the first region in terms of the wavenumber range and the growth rate of the disturbances. This region is not seen when the surface tension is neglected $(W = 0)$ and thus it can be concluded that the sole cause of this instability is the inclusion of surface tension at the interface with a piecewise-linear profile. Adding

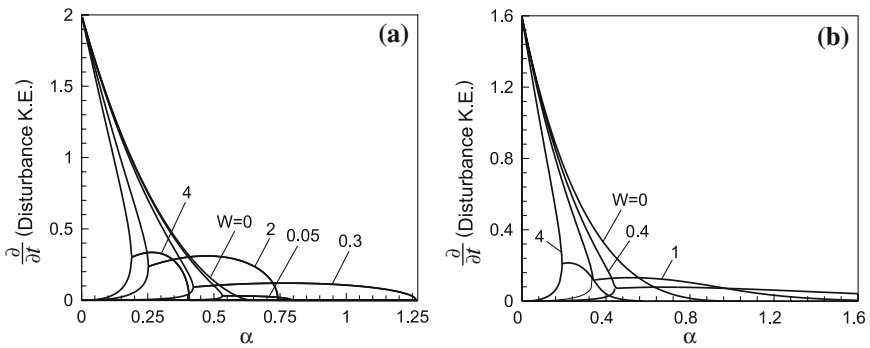

Figure 3. Temporal variation of the dimensionless disturbance kinetic energy vs. the dimensionless wavenumber for a homogeneous shear layer at different surface tension values. (a) Piecewise-linear profile, (b) error-function profile.

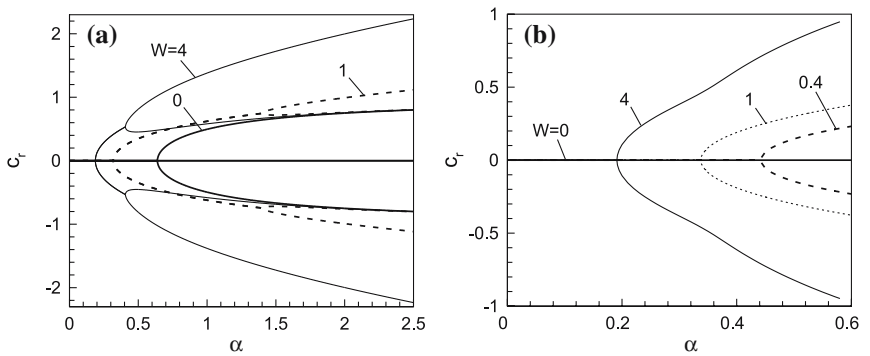

Figure 4. Dimensionless phase speed c_r vs. the dimensionless wavenumber α for a homogeneous shear layer at different surface-tension values. (a) Piecewise-linear profile, (b) error-function profile.

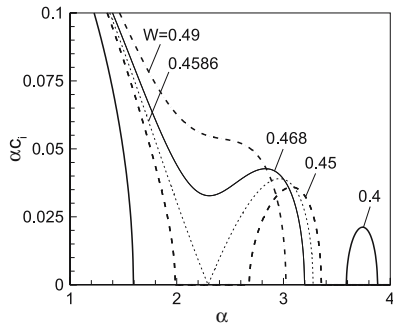

Figure 5. Dimensionless disturbance growth rate αc_i vs. the dimensionless wavenumber α for a homogeneous piecewise-linear profile with different surface tension values: the second unstable region.

a very small amount of surface tension creates an infinitesimal second unstable region at very short wavelengths. Increasing the surface tension would rapidly move the second region towards the first one while increasing its growth rate. The second region, however, does not persist for all W values. Figure 5 shows that at a particular value of W ($W_m = 0{\cdot}4586$) the two regions merge together to form one unstable region and only this merged region exists thereafter. That value is found to decrease monotonically when a density differential is imposed at the interface. However, this feature was not observed when a smooth velocity profile is considered for the mean flow. Figure 6(a) shows that the error-function profile has a continuous spectrum of unstable wavenumbers with only one cut-off which is close to the cut-off of the second region in the linear-profile case. The nature of the piecewise-linear profile structure is definitely what causes the unstable wavenumbers spectrum to split into two discontinuous regions. The linear profile is thus not a good approximation for a free shear-layer flow especially in the short-wave range. However, it can provide adequate results for long and intermediate wavelengths as it shows a good agreement with the error-function profile in that wavelength range, as shown in Figure 6(a). It should be pointed out that this is true even when surface tension is neglected. Figure 6(b) demonstrates that even when $W = 0$, the instability prediction of the short wavelength by the piecewise-linear profile does not agree with the one obtained with the error-function profile.

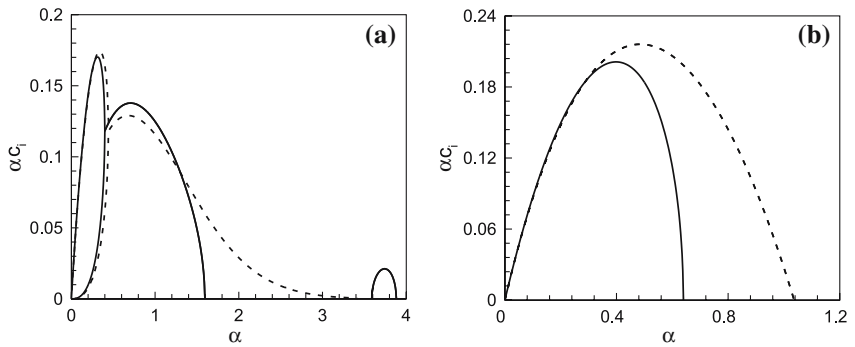

Figure 6. Comparison between the dimensionless growth rate αc_i of the piecewise-linear profile (solid line) and the error-function profile (dash line) for a homogeneous shear-layer flow. (a) $W = 0{\cdot}4$, (b) $W = 0$.

7.1.1. *Limit of very thin viscous layer*
In the limit of very thin viscous layer, that is $\delta \to 0$, Equation (20) reduces to:

$$c^2 = \tfrac{4}{3}\alpha\,(1-\alpha) \pm \tfrac{\sqrt{7}}{3}\alpha\left(1 - \tfrac{16}{7}\alpha\right). \tag{42}$$

To study the limit of small viscosity, consider Kelvin-Helmholtz instability, for instance, at $W = 100$. The cut-off wavenumber is found at 0·02. The corresponding values of c^2 for the piecewise-linear profile at $W = 100$ and $\alpha = 0{\cdot}02$ are:

$$c^2 = 0{\cdot}0430 \quad \text{and} \quad 0{\cdot}0093. \tag{43}$$

Hence, we conclude that a small amount of viscosity stabilizes all Kelvin-Helmholtz waves.

7.1.2. *Limit of infinite shear-layer thickness*
In the limit of infinite viscous layer or infinite wavenumber, that is $\delta \to \infty$ and $\alpha \to \infty$, Equation (20) reduces to:

$$c^2 = \frac{\alpha W}{2}, \tag{44}$$

which implies that the flow is then stable to all waves. When surface tension is ignored, the stable waves travel with the same speed of the interface, *i.e.*, stationary waves. If we assume that the wavenumber is very large ($\alpha \gg 1$) but finite, then Equation (20) can be written as:

$$c^2 = \begin{cases} \tfrac{1}{2}\alpha W \\ \left(1 - \tfrac{1}{2}\alpha^{-1}\right)^2 \end{cases}. \tag{45}$$

Again the flow is stable to all wavelengths in the range of $\alpha \gg 1$. For example, at $W = 0$ we have two set of stable waves. The first set travels with the interface and the other one travels with an asymptote to 1 and -1. It is worthwhile to mention that this result is valid for all $\alpha \gg 1$ regardless of the shear layer thickness.

7.2. Effect of background viscosity ($s = 1, m \neq 1$)

Although this work deals with the inviscid stability problem of free-shear-layer flows, viscosity does appear in an indirect manner through its effect on the background flow and therefore has a significant impact on the stability characteristics of the flow. In this section, we examine the effect of the background viscosity on the stability. First we investigate the effect of viscosity in the absence of surface tension, then when surface tension is taken into account. Since we are here interested only in the viscosity effect, the two streams are assumed to have the same density, *i.e.*, $s = 1$, throughout the analysis.

7.2.1. *No surface tension ($W = 0$)*
First we consider the cases when the lower fluid is more viscous than the upper one. We must keep in mind that, in our inviscid analysis, the effect of viscosity appears through its effect on the background velocity profile only. Figure 7 shows that the homogeneous shear layer has the least instability whereas the flow becomes more unstable with decreasing the viscosity ratio as the velocity profile in the upper fluid gets steeper. However, disturbances respond differently as we vary the viscosity ratio. Figure 8(a) shows that for a piecewise-linear profile, disturbances of small wavenumber ($\alpha < 0{\cdot}1$) are less sensitive to the viscosity ratio (the growth

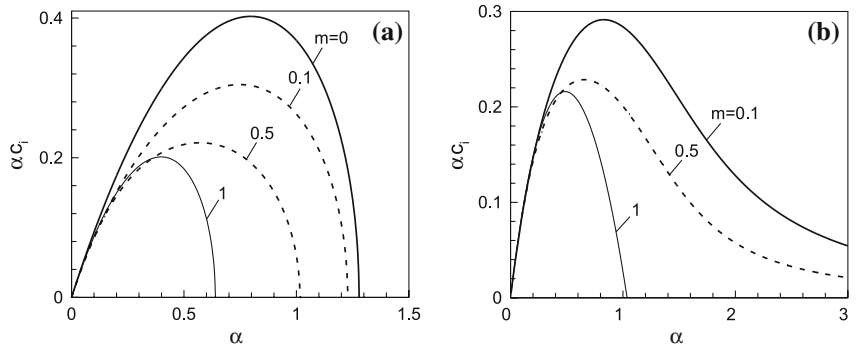

Figure 7. Dimensionless disturbance growth rate αc_i vs. the dimensionless wavenumber α for a same-density shear layer at various viscosity ratios ($m < 1$) and zero surface tension ($W = 0$). (a) Piecewise-linear profile, (b) error-function profile.

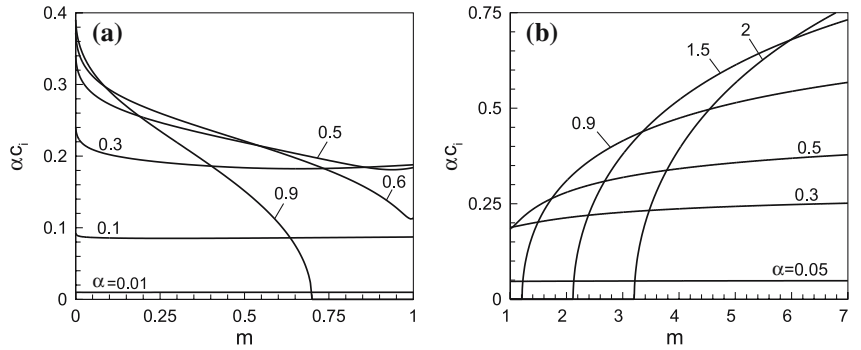

Figure 8. Dimensionless disturbance growth rate αc_i for a same-density piecewise-linear profile versus the viscosity ratio m at various dimensionless wavenumbers and $W = 0$. (a) $m < 1$, (b) $m > 1$.

rate is almost constant through the range of $m < 1$). On the other hand, for disturbances with large wavenumbers ($\alpha > 0{\cdot}5$), the destabilizing effect associated with increasing viscosity is significantly more noticeable. At the range of intermediate wavenumbers ($0{\cdot}1 < \alpha < 0{\cdot}5$), disturbances are observed to experience a slight damping as we increase the viscosity ratio when $m < 0{\cdot}1$.

The zero viscosity ratio ($m = 0$) curve in Figure 7(a) was obtained by taking the limit of $m \to 0$ for (19) and then substituting them in (18) taking $s = 1$ and $W = 0$. In this case, the quartic equation obtained in Section 5 reduces to the following cubic equation:

$$c^3 + c^2 + \left[\frac{2}{\alpha} - \frac{2\sinh\alpha}{\alpha^2 e^{\alpha}} - 1\right](c+1) = 0 \tag{46}$$

A very interesting property of this limit was observed. The growth rate of the most amplified wave in the limit of $m = 0$ is found to be twice (to 6 significant figures) that for $m = 1$ (0·402371 vs. 0·2011855). Furthermore, the optimum wavenumber at which the maximum instability occurs and the cut-off wavenumber for the flow with zero viscosity ratio are 0·796812 and 0·398406, respectively, which are greater than the corresponding wavenumbers for a uniform viscosity flow by a factor of two. This result is not surprising since, unlike the other cases, the velocity profiles for $m = 0$ and $m = 1$ possess a continuous slope across the interface and the velocity slope for the latter case is exactly half the one for the former one. Thus, the greatest instability the flow can reach by increasing the viscosity of the lower

fluid cannot exceed a value equal to twice the instability of the homogenous shear-layer flow. However, it should be pointed out that, besides these two cases, there is another case where the slope of the velocity maintains the same value as we cross the interface of the shear-layer. This occurs when the viscosity of the lower fluid approaches zero, in other words, when $m \to \infty$. In this case, the velocity profile has an infinite slope which makes the flow unstable to all wavelengths. It is worthwhile to mention that in the limit of $m \to \infty$, the background velocity recovers the inviscid problem of an infinite surface of discontinuity (vortex-sheet) where the flow becomes unstable to all wave lengths and hence the results of the Kelvin-Helmholtz instability can be used.

Next we examine the case when the lower fluid is less viscous than the upper one. From Figure 9 it can be seen that the degree of instability always grows with increasing viscosity difference. When the lower fluid is less viscous, its layer thickness decreases and the slope of the background velocity profile increases and this generates more instability.

Figure 8(b) illustrates the disturbance behavior for a piecewise-linear profile at large viscosity ratio range ($m > 1$). The disturbances show the same trend observed in the small m range as the long waves ($\alpha < 0{\cdot}1$) are unaffected by the change in the viscosity ratio. As opposed to the solution with long waves, short disturbed waves ($\alpha > 0{\cdot}6$) are affected by the viscosity ratio. These disturbances experience a substantial amplification as m increases. Note that the disturbed waves with the error-function profile do not differ from the linear profile in this respect.

The results obtained with the piecewise-linear profile again show significant disagreement when compared with the more accurate error-function profile. Figure 10 demonstrates this disagreement as it is more evident for shorter waves. Furthermore, the piecewise-linear profile becomes less realistic when the two fluids have different viscosity. For example at $m = 1{\cdot}5$, the linear profile yields stable waves beyond $\alpha = 1{\cdot}13$, while the error-function profile results in a flow that is not be stable before $\alpha = 10$.

7.2.2. *Effect of surface tension ($W = 5$)*

In general, a viscous background profile in the presence of surface tension is found to yield the same result on the stability characteristics of the same viscous profile in the absence of surface tension. However, it is worthwhile to point out some modifications on the disturbance behavior that are produced by the inclusion of surface tension.

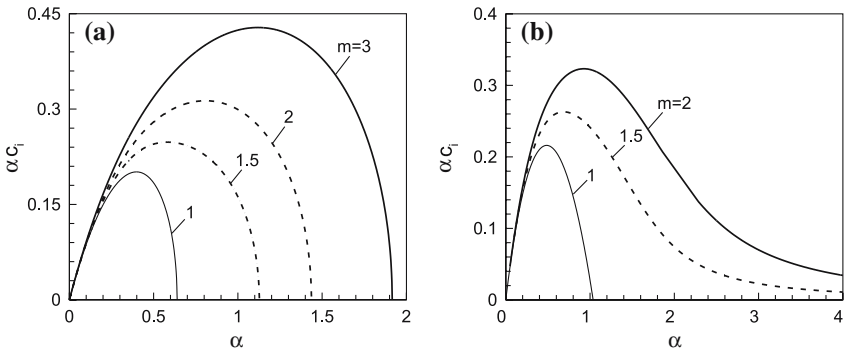

Figure 9. Dimensionless disturbance growth rate αc_i vs. the dimensionless wavenumber α for a same-density shear layer at various viscosity ratios ($m > 1$) and zero surface tension ($W = 0$). (a) Piecewise-linear profile, (b) error-function profile.

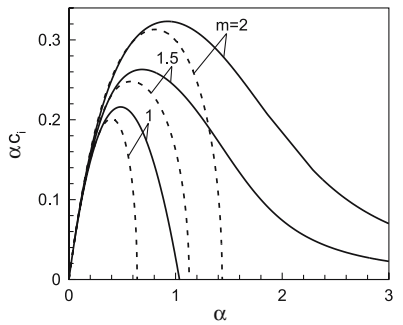

Figure 10. Comparison between the dimensionless growth rate αc_i of the piecewise-linear profile and the error-function profile for a same-density shear-layer flow at different viscosity ratios greater than one and $W = 0$.

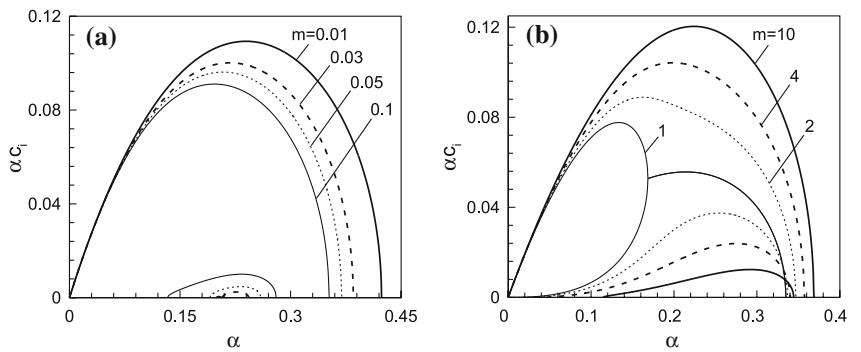

Figure 11. Dimensionless disturbance growth rate αc_i vs. the dimensionless wavenumber α for a same-density piecewise-linear profile at various viscosity ratios and $W = 5$. (a) $m < 1$, (b) $m > 1$.

As mentioned in Section 7.1, surface tension creates a second unstable mode which merges with the first mode if the flow is homogeneous, or which exists separately if the two streams have different properties. Figure 11 shows the effect of the background viscosity difference on these two modes. Decreasing the viscosity of the lower fluid stabilizes all disturbances in the first mode, but the opposite effect occurs on those disturbances of the second mode. A reduction in the viscosity of the lower fluid results in an enhancement of the amplification rate of the waves propagating through the second mode. This destabilizing effect of viscosity, however, is insignificant as far as the stability criteria are concerned, because only disturbances with larger growth rate, *i.e.*, first mode, are relevant when assessing the overall stability of the shear-layer flow. The viscosity ratio is still found to affect only the small and intermediate wavelengths ($\alpha > 0{\cdot}1$) while that effect is generally negligible for long waves even in the presence of surface tension.

Overall it can be concluded that the most stable state the shear-layer flow can reach is when both fluids have the same viscosity regardless whether surface tension is taken into account or not. Any variation in the background viscosity from that homogeneity status will definitely result in more instability.

7.3. Nonhomogeneous shear flow ($s = m \neq 1$)

In this section we examine the stability of a background flow that consists of two fluids of different density and viscosity but equal kinematic viscosity. The ratio between the kinematic viscosity of the upper and lower stream equals the ratio between m and s. From the similarity solution for a free shear-layer flow [16, Section 4.3], this ratio can be expressed in terms

of the shear-layer thickness:

$$\frac{\nu_1}{\nu_2} = \frac{m}{s} = \left(\frac{\delta_1}{\delta_2}\right)^2. \tag{47}$$

Thus the $s = m \neq 1$ case, implies that the two streams have the same shear-layer thickness.

It can be seen from Figure 12 that imposing a density and viscosity difference across the interface of the shear flow causes the second mode, created by the surface tension, to be detached from the first mode and hence the wavenumber at which both modes merge, α_m, that was observed in the homogeneous shear flow does not exist and the second mode now has its own cut-off wavenumber. This behavior, however, does not necessarily require a discontinuity in both the density and viscosity across the interface. It is enough to have two fluids with different density or viscosity as seen in Section 7.2. Furthermore, as we increase the difference in the density and viscosity between the two fluids, the second mode becomes even more independent and extremely less evident compared with the first mode at larger surface tension.

In Section 7.1 surface tension was found to create a second unstable region for the piecewise-linear profile after a certain range of stable wavenumbers. When the two fluids, in the presence of surface tension, are of different density and (or) viscosity, the flow experiences a third unstable zone. Figure 13 demonstrates this behavior clearly where the first and second spike in each curve represent, respectively, the second and third unstable region except for the homogeneous flow case where only the second region exists.

The same observation regarding the validity of the piecewise-linear profile that was made in Section 7.1 is made here. Figure 14 shows that for an error-function profile with $s = m = 0{\cdot}3$ and $W = 2{\cdot}33$ the unstable wavenumbers spectrum is continuous in contrast with the results obtained for the piecewise-linear profile, which has two distinguished unstable wavenumbers regions. Although the second mode solution for the linear profile shows a good agreement with the error-function, the solution of the first mode, which is more important, does not match the one obtained with the error-function profile. Furthermore, Figure 14 shows that the long-wavelength disturbances are not affected by the structure of the velocity profile. Physically, the waves start to respond to the structure of the profile appreciably when the dimensional wavenumber is of the same or larger order than the shear-layer thickness. Since we used the shear-layer thickness as the characteristic length, then we expect this will occur when the dimensionless wavenumber is equal or larger than 1.

When surface tension is neglected, the error-function profile with equal density and viscosity ratios exhibits a very interesting behavior. Figure 15(a) shows that all instability curves

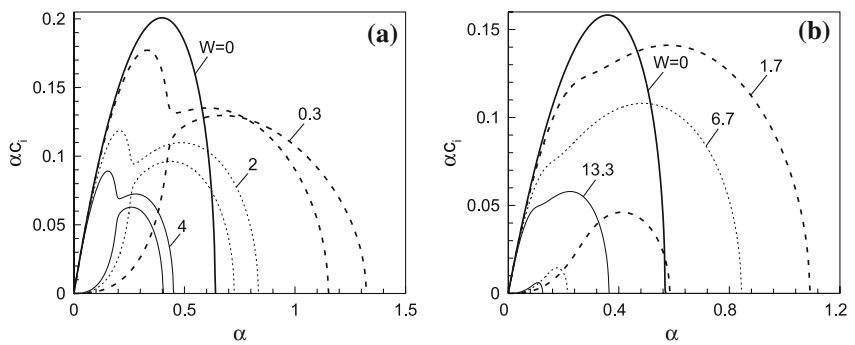

Figure 12. Dimensionless disturbance growth rate αc_i vs. the dimensionless wavenumber α for a piecewise-linear profile at different W values. (a) $s = m = 0{\cdot}9$, (b) $s = m = 0{\cdot}3$.

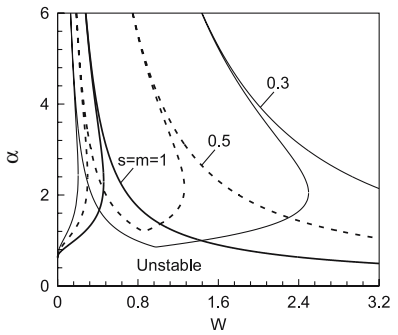

Figure 13. Neutral stability curves for a piecewise-linear profile at different $s = m$.

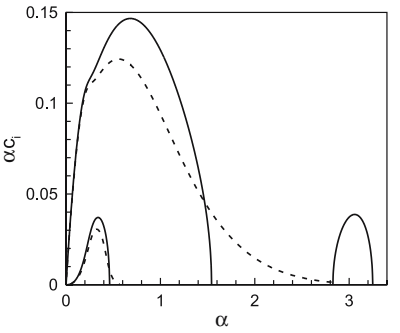

Figure 14. Comparison between the dimensionless growth rate αc_i of the piecewise-linear profile (solid line) and the error-function profile (dash line) for a shear-layer flow with $s = m = 0{\cdot}3$ and $W = 2{\cdot}33$.

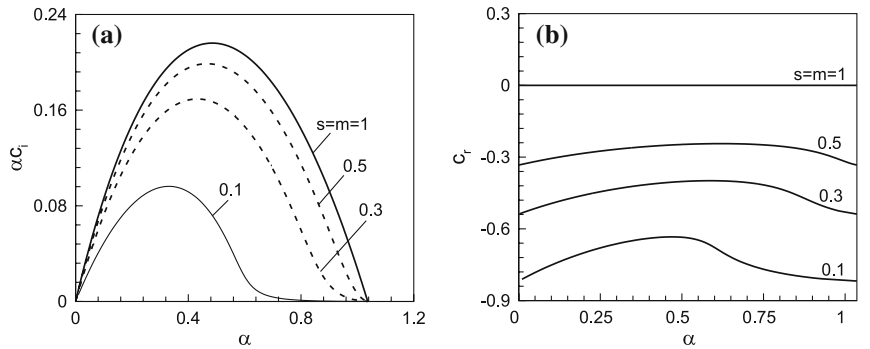

Figure 15. Error-function profile with $W = 0$ at various $s = m$ values. (a) Growth rate αc_i, (b) phase speed c_r.

have the same cut-off wavenumber α_c regardless of the value of the density and viscosity ratios. This cut-off is found to be 1·036. To understand the reason behind this behavior, it is important to study the phase speed of these disturbances which is shown in Figure 15(b). It can be seen that the phase speed of all the cases always approaches the interface velocity at the cut-off. This behavior makes the differential equations in (30) and (31) independent of s and m at the cut-off wavenumber, which in turn makes the solution to these equations produces the same cut-off as long as $W = 0$.

8. Conclusions

The inviscid temporal instability of an unbounded shear layer of two fluids of different density is investigated by performing a full linear stability analysis. The viscosity of the background flow is incorporated through the velocity profiles of the background flow. Two background velocity profiles were examined: the piecewise-linear profile and the more realistic error-function profile. A quartic dispersion equation is derived analytically for the former, while the eigenvalues for the latter are computed numerically with the aid of a new optimization technique. A detailed study of the kinetic energy of inviscid disturbances is carried out to physically understand the mechanisms of instability.

The surface-tension effects are emphasized. Apart from the stabilizing effect observed in most of the cases, surface tension is found to destabilize the neutrally stable waves that exist

when the interfacial tension is absent. This second unstable mode is independent of the first (stronger) mode and extremely less evident when the background viscosity and/or density difference increases. It is shown that short waves are destabilized by a small amount of surface tension. This destabilizing effect of surface tension can be attributed to the additional discontinuity in the tangential velocity at the interface caused by surface tension. From a mathematical point of view, surface tension is found to shift the phase angle difference of the perturbation velocities outside the stable quadrants. This shift leads to a positive Reynolds stress which is large enough to overcome the otherwise stabilizing effect of surface tension and rendering these otherwise neutrally stable waves unstable.

Increasing the background viscosity difference through the background velocity profile gives rise to short wavelength instability and the flow is most unstable in the limit of background viscosity ratio $m = 0$. Interestingly, the growth rate of the most amplified wave in this limit is found to be twice that for $m = 1$. Furthermore, the optimum wavenumber at which the maximum growth rate occurs and the neutrally stable wavenumber of $m = 0$ are greater than the corresponding wavenumbers for a uniform viscosity flow by a factor of two.

A comparison between the two velocity profiles is presented. The piecewise-linear profile does not match the more realistic results obtained with the error-function profile in the short wavelength range, especially in nonhomogeneous shear-layer flows. However, the phase speed results are in a good agreement with those of the error-function profile.

References

1. R.E. Esch, The instability of a shear layer between two parallel streams. *J. Fluid Mech.* 3 (1957) 289–303.
2. J.W. Miles, On the generation of surface waves by shear flows. Part 3. *J. Fluid Mech.* 7 (1959) 583–598.
3. K.A. Lindsay, The Kelvin–Helmholtz instability for a viscous interface. *Acta Mech.* 52 (1984) 51–61.
4. R.G. Zalosh, Discretized simulation of vortex sheet evolution with buoyancy and surface tension effects. *AIAA J.* 14 (1976) 1517–1523.
5. R.H. Rangel and W.A. Sirignano, Nonlinear growth of Kelvin-Helmholtz instability: Effect of surface tension and density ratio. *Phys. Fluids* 31 (1988) 1845–1855.
6. P.G. Drazin and L.N. Howard, The instability to long waves of unbounded parallel inviscid flow. *J. Fluid Mech.* 14 (1962) 257–283.
7. A. Michalke, On the inviscid instability of the hyperbolic-tangent velocity profile. *J. Fluid Mech.* 19 (1964) 543–556.
8. R.V. Garcia, Barotropic waves in straight parallel flow with curved velocity profile. *Tellus* 8 (1956) 82–93.
9. T. Tatsumi, K. Gotoh and K. Ayukawa, The stability of a free boundary layer at large Reynolds numbers. *J. Phys. Soc. Jpn.* 19 (1964) 1966–1980.
10. O. Pouliquen, J.M. Chomaz and P. Huerre, Propagating Holmboe waves at the interface between two immiscible fluids. *J. Fluid Mech.* 266 (1994) 277–302.
11. L.G. Redekopp, Elements of instability theory for environmental flows. In: R. Grimshaw *et al*. (eds.), *Environmental Stratified Flows*. Kluwer Academic Publishers (2002) pp. 223–81.
12. P.G. Drazin and W.H. Reid, *Hydrodynamic Stability*. 2nd ed. New York: Cambridge University Press (1981) 525 pp.
13. L. Prandtl, The mechanics of viscous fluids. In: W.F. Durand (ed.), *Aerodynamic Theory*. Berlin: J. Springer (1935) pp. 34–208.
14. T. Tatsumi and K. Gotoh, The stability of free boundary layers between two uniform streams. *J. Fluid Mech.* 7 (1960) 433–441.
15. C.-S. Yih, Instability due to viscosity stratification. *J. Fluid Mech.* 27 (1967) 337–352.
16. F.M. White, *Viscous Fluid Flow*. 2nd ed. New York: McGraw-Hill (1991) 614 pp.